

# CFCamo: A Counterfactual Detect-or-Abstain Framework for Camouflaged Object Detection

Suhang Li, Osamu Yoshie, and Yuya Ieiri

**Abstract**—Vision-language reinforcement learning has recently shown strong target-present localization for camouflaged object detection (COD). Yet localization is only one side of the decision: when the agent faces an ordinary image with no camouflaged target, will it still claim that a camouflaged object exists? Standard COD training and evaluation data are positive-only, so agents optimized under this setting can acquire an over-detect bias, a task-specific form of object hallucination that standard COD evaluation leaves unmeasured. To quantify this target-absent behavior, we construct Counterfactual COD (CF-COD), a paired benchmark that removes the camouflaged target from each held-out COD evaluation image while preserving a plausible background. CF-COD evaluates whether a model detects the target on the original image and abstains on the target-absent counterfactual, summarized by Pair Accuracy (PA). We further introduce CFCamo, a paired counterfactual framework for COD with abstention. For training, CFCamo optimizes a Qwen3-VL-4B-Instruct agent with Counterfactual Sequence Policy Optimization (CSPO), which samples paired original-counterfactual rollouts and uses a Counterfactual Paired Reward (CPR) to couple original-image detection with counterfactual abstention. On CAMO-test, CFCamo improves  $S_\alpha$  by +3.7 pp over the prior RL-based COD baseline; across CF-COD, it reaches 80.0–90.8% PA. Ablations show that removing counterfactual coupling reduces PA to 1.4–5.2% despite strong target-present COD scores, showing that target-present evaluation alone does not characterize detect-or-abstain behavior. Overall, these results indicate that CFCamo improves COD agents by coupling target-present detection with target-absent abstention, rather than merely strengthening target-present localization. Code and data are available at <https://github.com/suhang2000/CFCamo>.

**Index Terms**—Camouflaged object detection, vision-language model, reinforcement learning, counterfactual reasoning.

## I. INTRODUCTION

CAMOUFLAGE is a widespread biological survival strategy in which organisms evolve appearance that blends into their surroundings to evade detection [1], [2]. Camouflaged object detection (COD) [3], [4] aims to localize and segment such targets that visually merge with complex backgrounds. Unlike salient object detection on visually prominent targets, COD must operate when the target’s local appearance contrast with the background is minimized. Related low-contrast segmentation settings arise in medical image analysis (e.g., polyp segmentation [5]), biological and ecological studies [6], and industrial visual inspection (e.g., surface-defect detection [7]). Early COD systems rely on dense-prediction networks supervised by pixel masks [8]–[11]. A recent line of work reformulates COD as visual grounding for a vision-language model (VLM): the model emits spatial prompts and

a frozen SAM-style decoder [12], [13] turns them into a mask. Seg-R1 [14] further trains such a VLM by reinforcement learning (RL) with a mask-level reward and reports strong COD scores.

As illustrated in Fig. 1, strong target-present accuracy can hide a deployment-relevant failure mode: *over-detect bias*, a spatial form of object hallucination in which the agent claims a camouflaged target where none is present. In real-world applications, many inputs are ordinary target-absent scenes, and repeated false alarms on such backgrounds reduce deployment reliability. However, standard COD training and evaluation benchmarks are positive-only: each image is assumed to contain at least one camouflaged target. A VLM trained under this distribution can therefore learn a prior of issuing a detection whenever it receives a COD prompt, while standard COD evaluation does not test the target-absent case. For example, on target-absent counterfactuals synthesized by ObjectClear inpainting, even with an explicit abstention token in the prompt, our re-run of Seg-R1-7B [14] still emits a bounding box on 38% of COD10K-test images (Fig. 1). This behavior indicates target-present predictions in the absence of target evidence, rather than decisions conditioned only on what remains visible in the scene.

To address over-detect bias, we propose CFCamo, a paired detect-or-abstain COD agent optimized using Counterfactual Sequence Policy Optimization (CSPO). Instead of optimizing target-present inputs in isolation, CSPO operates on original-counterfactual image pairs and enforces a coupled Counterfactual Paired Reward (CPR) that scores the joint decision rather than the two scenarios independently. This formulation couples positive detection with negative abstention in a single RL objective, so indiscriminate detection no longer gives high reward. To systematically diagnose this capability, we construct Counterfactual COD (CF-COD), a paired diagnostic benchmark generated by a frozen inpainting model [15]. Each evaluation image is paired with its target-absent counterfactual, and Pair Accuracy (PA) measures whether the model detects on the original image and abstains on the counterfactual. Trained on a Qwen3-VL-4B-Instruct [16] backbone, CFCamo substantially reduces over-detection on CF-COD, improves standard COD performance against task-generic prompt baselines, and keeps general multimodal capability close to the base model.

Our contributions are as follows.

- We propose Counterfactual Sequence Policy Optimization (CSPO), a paired-counterfactual reinforcement learning framework to mitigate over-detect bias in vision-language models. By integrating paired-counterfactual rollouts and a sequence-level importance ratio under a

The authors are with the Graduate School of Information, Production and Systems, Waseda University, Fukuoka, Japan.

Corresponding author: Osamu Yoshie (e-mail: yoshie@waseda.jp).

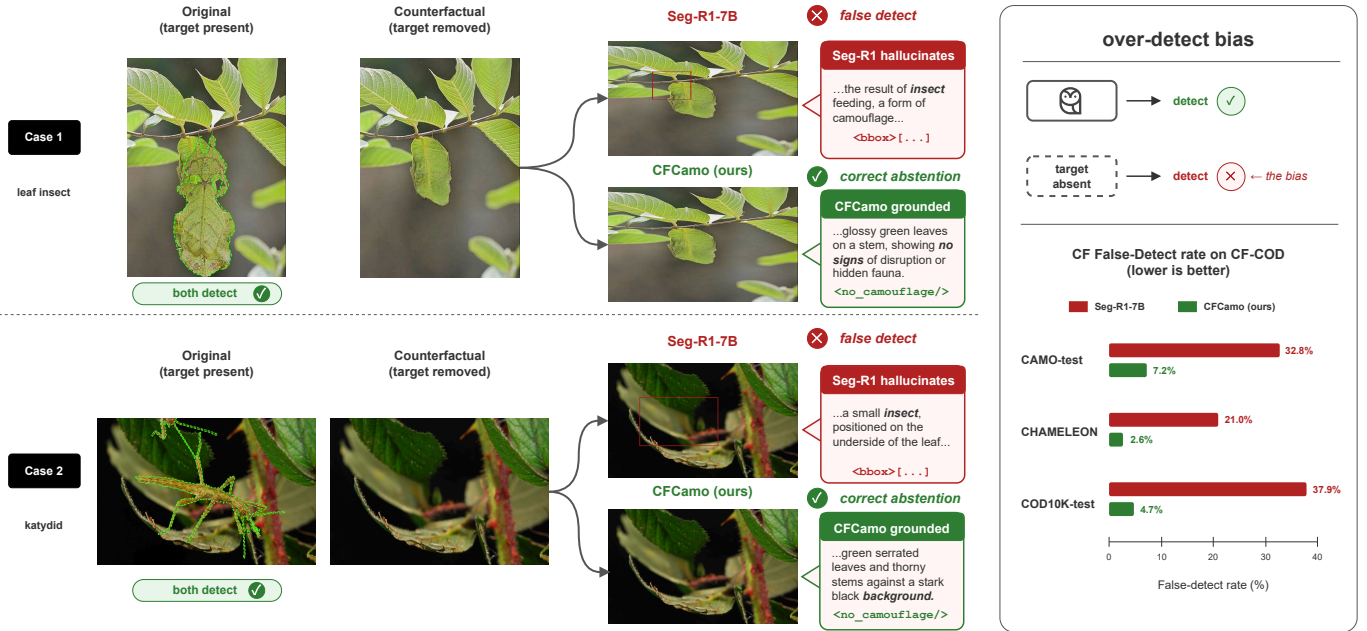


Fig. 1. Motivation of CFCamo and CF-COD. Standard COD benchmarks evaluate target-present images, whereas deployment also contains target-absent scenes. In each paired (original, target-absent) example, Seg-R1-7B still predicts a box on the target-absent counterfactual, whereas CFCamo detects the original target and correctly abstains. Right: false-detect rates on CF-COD counterfactuals (lower is better).

coupled Counterfactual Paired Reward (CPR), CSPO optimizes a single policy to jointly detect targets on original images and abstain on target-absent counterfactuals.

- We construct the Counterfactual COD (CF-COD) benchmark, a paired evaluation framework for camouflaged object detection that scores joint correctness on original-counterfactual pairs and makes over-detect bias directly measurable.

## II. RELATED WORK

### A. Camouflaged Object Detection

Camouflaged object detection (COD) localizes objects whose appearance is intentionally or naturally blended into the surrounding scene [17] [3]. The dominant paradigm trains dedicated dense-prediction networks under pixel-level supervision, with many mechanisms proposed to handle the appearance ambiguity of camouflaged targets. PFNet mines distractor regions to suppress confusing backgrounds [8], and BGNet uses object boundaries as auxiliary supervision to sharpen target contours [9]. To recover textures missed by the spatial branch, FGSA-Net introduces frequency-domain guidance into the spatial adaptation of a pretrained backbone [18]. HitNet iteratively refines low-resolution predictions with high-resolution features to avoid detail loss [10], and ZoomNeXt integrates multi-scale feature interactions in a collaborative pyramid [11]. UGDNet casts COD as iterative denoising under an explicit uncertainty condition [19].

Another line repurposes the Segment Anything Model family [12] [13] as a mask decoder driven by external prompts. GenSAM removes the per-image prompt requirement by deriving visual prompts from a single generic text prompt with cross-modal chain-of-thought prompting [20]. ProMaC turns

a multimodal LLM’s hallucinations into candidate prompts, refined through a prompt-mask cycle where an inpainter generates background-only contrastive images to filter co-occurrence hallucinations at inference time [21]. RDVP-MSD couples a multimodal stepwise chain of thought for caption disambiguation with region-constrained, dual-stream prompt sampling for foreground and background [22]. Beyond these training-free pipelines, Seg-R1 trains an RL agent that emits spatial prompts directly from the image [14]. CFCamo formulates COD as a paired detect-or-abstain problem, and trains the detector with a pair-level reward over the original image and its inpainted counterfactual, so that explicit abstention on target-absent scenes becomes a learned, first-class output.

### B. Vision-Language Models for Pixel-Level Understanding

A broader line of work extends large multimodal models (LMMs) to pixel-level output. LISA [23] first introduced a dedicated `<SEG>` token that aligns an LMM with a mask decoder. GLaMM extends this recipe to grounded multi-object conversation with region-level captioning [24]. PixelLM replaces the mask decoder with a lightweight pixel-token codebook [25]. OMG-LLaVA unifies image-, object-, and pixel-level understanding in a single LMM [26]. SESAME teaches an LMM to verify referent existence before segmenting, enabling abstention on false-premise referring queries [27].

Another line applies reinforcement learning to prompt-based segmentation, building on Group Relative Policy Optimization (GRPO) [28]. Seg-Zero [29] freezes SAM2 and rewards only the geometric prompts (bounding box and points), whereas Seg-R1 [14] additionally feeds the SAM2-decoded mask back into the reward as a mask-quality signal. SAM-R1 [30] tightens this loop with tiered segmentation-accuracy rewards driven

by SAM2; VisionReasoner [31] unifies detection, segmentation, and counting under a Hungarian-matched multi-object reward; and LENS [32] fine-tunes the MLLM and the SAM2 mask decoder while keeping the segmentation image encoder fixed. CFCamo extends this paradigm to camouflaged object detection: the per-image reward is replaced by a pair-level reward over an original image and its inpainted counterfactual, which couples detection and abstention in a single training objective.

### C. Counterfactual Reasoning for Vision-Language Model Hallucination

A separate body of work studies vision-language model hallucination through object probing, paired comparisons, or counterfactual inputs. Several benchmarks target different aspects: POPE [33] queries object existence with polling-style questions, BEAF [34] evaluates the model on paired before-after object removal, and HaloQuest [35] covers multiple hallucination types. Among mitigation methods, REVERSE [36] suppresses visual hallucination through hallucination-verification data and retrospective resampling, and PAPO [37] adds an implicit perception KL between policy distributions conditioned on the original versus a corrupted visual input to enforce visual grounding.

HalluSegBench [38] constructs a paired benchmark for pixel-grounding hallucination under counterfactual object substitution. CIPHER [39] suppresses vision-induced LVLM hallucination by projecting hidden states away from an offline hallucination subspace learned from diffusion-edited counterfactuals, all at inference time. Visual Jenga [40] uses counterfactual inpainting in a training-free manner to quantify pairwise object dependencies. CFCamo applies counterfactual inpainting at training time for camouflaged object detection, exploiting a task-specific property: a target-absent counterpart of a camouflaged scene is simply a natural background image, easier to acquire than the camouflaged scene itself. We pair such counterparts with the originals and supervise them with a pair-level reinforcement-learning reward, so the model learns both to localize camouflaged targets and to abstain on natural scenes.

## III. METHOD

CFCamo reframes camouflaged object detection from a positive-only localization problem into a paired detect-or-abstain problem (Fig. 2). Standard COD pipelines assume that a camouflaged object is always present, so a vision-language detector earns reward simply by emitting a box on every input. This assumption does not hold on counterfactual scenes that contain no camouflaged object even though the background remains plausible: an empty scene should not receive a detection box, otherwise the policy defaults to an over-detect strategy. CFCamo addresses this by optimizing a single VLM policy to localize on original COD images and to abstain on their inpainted counterfactuals, within one output space.

Concretely, CFCamo extends Group Sequence Policy Optimization (GSPO) [41] along three axes, which together

form Counterfactual Sequence Policy Optimization (CSPO): (i) a paired counterfactual rollout that draws  $G$  original and  $G$  counterfactual responses per pair (Section III-B); (ii) a Counterfactual Paired Reward (CPR) that couples original-image detection with counterfactual abstention via detection and abstention indicators and a pair-level coupling bonus (Section III-C); and (iii) a paired sequence ratio that extends GSPO’s length-normalized importance ratio jointly across each original-counterfactual pair (Section III-D).

### A. Problem Formulation

In the VLM-to-SAM formulation used here, a policy  $\pi_\theta : x \mapsto y$  emits a structured response whose terminal decision is converted into a mask by SAM2. For a target-present COD image  $x$  with ground-truth mask  $m$ , the desired terminal decision is a bounding box for the camouflaged object. CFCamo extends this setting to paired inputs  $(x_o, x_c)$ , where  $x_o$  is an original COD image and  $x_c$  is its target-absent counterfactual counterpart. Writing  $y_o = \pi_\theta(x_o)$  and  $y_c = \pi_\theta(x_c)$ , the desired behavior is asymmetric across the pair:

$$\begin{aligned} y_o &\rightarrow \text{detect (bbox)}, \\ y_c &\rightarrow \text{abstain}. \end{aligned} \quad (1)$$

Both responses begin with a `<think>...</think>` reasoning block. The detect output terminates in one or more bounding boxes, whereas the abstaining output terminates in the dedicated token `<no_camouflage/>`.

### B. Paired Training Data

**Counterfactual generation.** We generate counterfactual pairs for both training and evaluation: the CAMO/COD10K training pairs are used for SFT and CSPO, while CF-COD denotes the held-out paired evaluation suite. For training, we build the paired training set from the combined CAMO [17] and COD10K [3] training splits (4040 original images). For each original  $x_o$ , ObjectClear [15] fills the ground-truth mask region to produce a target-absent counterpart  $x_c$ . Compared with random negative sampling, this construction preserves background, illumination, and local texture, so abstention must be driven by the disappearance of the camouflaged evidence rather than dataset-level shortcuts.

**Cold-start supervised data.** Before reinforcement learning, we run a short SFT stage to teach the model the output schema and a basic reasoning style. We randomly sample 750 detect and 750 abstain examples to form the SFT pool; rationales for both response types are generated by an external language model (Gemini 3.1-flash-lite [42]) at temperature 0. The main setting uses the balanced 500/500 subset of this pool; other ratios are studied in Section V-A.

**Reinforcement-learning data.** The paired training set contains 4040 pairs in total, yielding 8080 rollout inputs per epoch (each pair contributes one rollout on  $x_o$  and one on  $x_c$ ). Our main model is trained for half an epoch, which covers roughly 2020 pairs ( $\approx 4040$  image-views), matching the size of the standard COD training set.

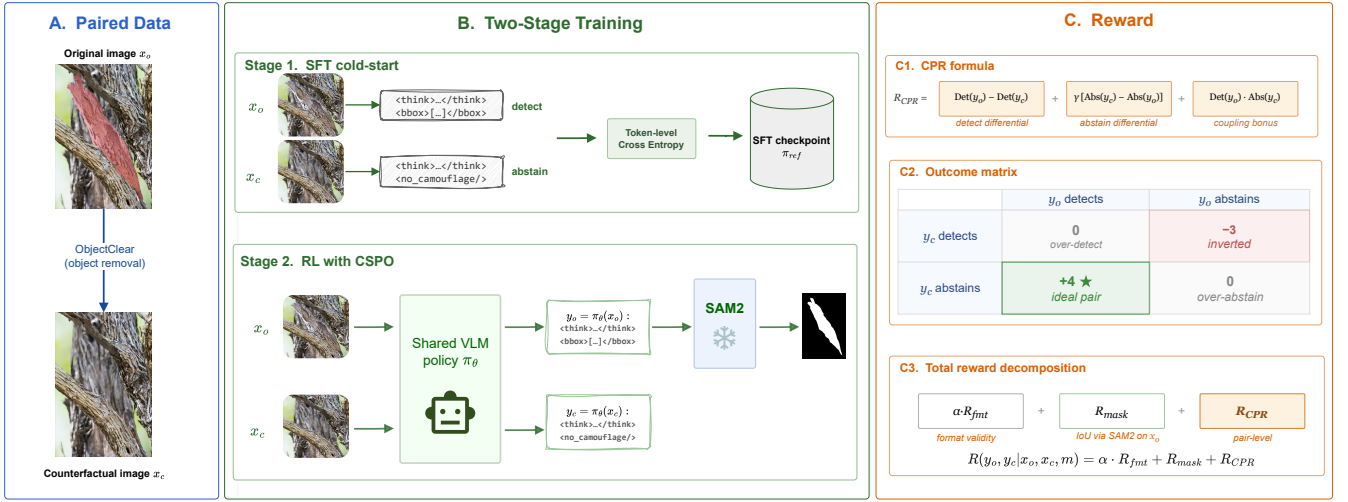


Fig. 2. Overview of the CFCamo framework. Paired training data  $(x_o, x_c)$  are formed by pairing  $x_o$  with a target-absent counterpart  $x_c$  from an off-the-shelf inpainter. Stage 1 cold-starts the VLM with a balanced supervised fine-tuning (SFT) corpus to teach the detect-or-abstain format. Stage 2 trains the VLM with CSPO; a frozen SAM2 decoder turns predicted boxes into masks for the reward’s mask-IoU term.

### C. Reward Design

The total reward over a paired sample  $(x_o, x_c)$  has three components: a mask-quality reward  $R_{mask}$ , a format-validity reward  $R_{fnt}$  with a small weight  $\alpha = 0.1$ , and our Counterfactual Paired Reward  $R_{CPR}$ ,

$$R(y_o, y_c | x_o, x_c, m) = \alpha R_{fnt} + R_{mask} + R_{CPR}. \quad (2)$$

The first two terms follow prior RL-based segmentation methods [14], [29];  $R_{CPR}$  ties detection on  $x_o$  to abstention on  $x_c$  in one reward, so no separate abstention head is required.

**Format and mask-quality rewards.** The format indicator  $\text{Fmt}(y) = 1$  if  $y$  has a well-formed reasoning block and ends with exactly one valid terminal decision (a bounding box or the abstention token `<no_camouflage/>`);  $\text{Fmt}(y) = 0$  otherwise. The format reward sums  $\text{Fmt}$  over the two responses,

$$R_{fnt}(y_o, y_c) = \text{Fmt}(y_o) + \text{Fmt}(y_c). \quad (3)$$

For the mask reward, we feed the predicted box into SAM2 [13] and score the resulting mask against the ground truth  $m$  on the original image. Letting  $\text{Det}(y) = 1$  if  $y$  contains a valid bounding box (and 0 otherwise) and  $\text{IoU}_o = \text{IoU}(\text{SAM2}(\text{bbox}(y_o), x_o), m)$ ,

$$R_{mask}(y_o, x_o, m) = \text{IoU}_o \cdot \text{Det}(y_o), \quad (4)$$

which is zero whenever  $y_o$  abstains or is malformed.

**Counterfactual paired reward.** On the counterfactual side, the abstention indicator  $\text{Abs}(y) = 1$  if  $y$  ends with the abstention token (and 0 otherwise).  $R_{CPR}$  then combines the four pair-level outcomes antisymmetrically through  $\text{Det}$  and  $\text{Abs}$ :

$$R_{CPR}(y_o, y_c) = \begin{aligned} &\text{Det}(y_o) - \text{Det}(y_c) && \text{(detect)} \\ &+ \gamma[\text{Abs}(y_c) - \text{Abs}(y_o)] && \text{(abstain)} \\ &+ \text{Det}(y_o) \text{Abs}(y_c). && \text{(coupling)} \end{aligned} \quad (5)$$

Each differential rewards the correct behavior on its side and penalizes it on the other: the over-detect bias appears as

the  $-\text{Det}(y_c)$  term, and over-abstention as  $-\text{Abs}(y_o)$ . The coupling bonus fires only on the ideal pair, adding a pair-level signal that per-image rewards alone cannot deliver.

We use  $\gamma = 2$  throughout. By antisymmetry, the two trivial strategies receive zero CPR: the detect differential  $\text{Det}(y_o) - \text{Det}(y_c)$  vanishes under over-detection, and the abstain differential  $\gamma[\text{Abs}(y_c) - \text{Abs}(y_o)]$  vanishes under over-abstention. The ideal pair receives the largest CPR value,  $1 + \gamma + 1 = 4$ , whereas the inverted abstain-detect pair receives  $-1 - \gamma = -3$ .

### D. Two-Stage Training

**Stage 1: Supervised fine-tuning.** We first fine-tune the base VLM on the cold-start data  $\mathcal{D}_{\text{SFT}}$  of Section III-B by minimizing the token-level cross-entropy

$$\mathcal{L}_{\text{SFT}}(\theta) = -\mathbb{E}_{(x, y^*) \sim \mathcal{D}_{\text{SFT}}} \sum_{t=1}^{|y^*|} \log \pi_\theta(y_t^* | y_{<t}^*, x), \quad (6)$$

where  $y^*$  is the supervised response (a reasoning block followed by a bounding box or the abstention token). This teaches the model the CFCamo response format before any reward is applied; the resulting checkpoint then initializes Stage 2 and serves as the reference policy  $\pi_{ref}$  for the KL anchor in Eq. (7).

**Stage 2: Reinforcement learning.** We then optimize the reward of Section III-C with CSPO, which follows the sequence-level clipped objective of GSPO [41], itself a sequence-level variant of GRPO [28]. For each pair  $(x_o, x_c)$  we sample  $G$  rollouts per side from the behavior policy  $\pi_{\theta_{old}}$ , pair them by index as  $o_i = (y_{o,i}, y_{c,i})$ , and score each pair with the total reward  $R(o_i)$  from Eq. (2). The policy maximizes

$$\mathcal{J}_{\text{CSPO}}(\theta) = \mathbb{E} \left[ \frac{1}{G} \sum_{i=1}^G \min(s_i \hat{A}_i, \text{clip}(s_i, 1-\epsilon, 1+\epsilon) \hat{A}_i) \right], \quad (7)$$

$$- \beta_{kl} D_{\text{KL}}(\pi_\theta \| \pi_{ref})$$

## CF-COD Benchmark

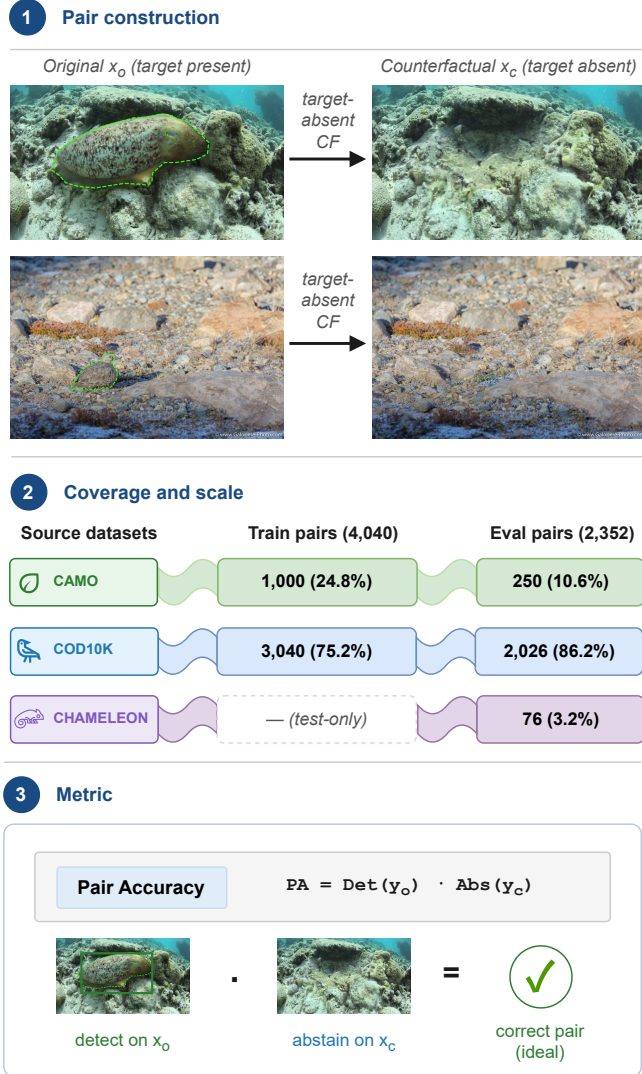


Fig. 3. Overview of the paired counterfactual data. Top: representative paired examples (original  $x_o$  with the target outlined vs. target-absent counterfactual  $x_c$ ). Middle: train/eval split (4,040 training pairs from CAMO/COD10K and 2,352 held-out evaluation pairs forming CF-COD, with CHAMELEON as test-only). Bottom: the Pair Accuracy scoring rule.

where the sequence-level ratio  $s_i$  extends GSPO to the matched pair as the length-normalized geometric mean of the joint likelihood ratio,

$$s_i = \left( \frac{\pi_{\theta}(y_{o,i} | x_o) \pi_{\theta}(y_{c,i} | x_c)}{\pi_{\theta_{\text{old}}}(y_{o,i} | x_o) \pi_{\theta_{\text{old}}}(y_{c,i} | x_c)} \right)^{1/(|y_{o,i}|+|y_{c,i}|)}, \quad (8)$$

which stabilizes training on variable-length reasoning trajectories.  $\hat{A}_i$  is the group-relative advantage normalized within  $\{R(o_1), \dots, R(o_G)\}$ ,  $\pi_{\text{ref}}$  is the SFT checkpoint, and  $\epsilon$  and  $\beta_{\text{kl}}$  are the clip threshold and KL coefficient.

Our main model fine-tunes all parameters under the half-epoch budget of Section III-B. We also train a low-rank adaptation (LoRA) variant as a compute-efficient alternative, used in our ablations.

## IV. EXPERIMENTS

### A. Experimental Setup

**Datasets.** Training uses the CAMO [17] (1,000 images) and COD10K [3] (3,040 images) train splits, totaling 4,040 images, each paired with an ObjectClear-inpainted, target-absent counterfactual. Testing covers three benchmarks: CAMO-test (250 images), CHAMELEON [43] (76 images), and COD10K-test (2,026 images); their held-out original-counterfactual pairs constitute CF-COD.

**Standard COD metrics.** Standard COD performance uses four metrics: (1) structure-measure  $S_{\alpha}$  [44], which captures structural similarity between prediction and ground truth in region-aware and object-aware ways; (2) enhanced-alignment measure  $E_{\phi}$  [45], which combines local pixel alignment with global statistics, with the mean score reported; (3) weighted F-measure  $F_{\beta}^w$  [46], which weights precision and recall toward perceptually significant errors; and (4) mean absolute error  $M$  [47], the average pixel-wise difference between the predicted and ground-truth masks. Higher is better for  $S_{\alpha}$ ,  $E_{\phi}$ , and  $F_{\beta}^w$ ; lower is better for  $M$ .

**CF-COD paired protocol.** For CF-COD pairs, using the per-sample predicates  $\text{Det}$  and  $\text{Abs}$  defined in Section III-C, we report Detection Rate  $D_o = \frac{1}{N} \sum_{i=1}^N \text{Det}(y_o^{(i)})$  on original COD images and Abstention Rate  $A_c = \frac{1}{N} \sum_{i=1}^N \text{Abs}(y_c^{(i)})$  on counterfactuals. The headline metric is the joint Pair Accuracy

$$PA = \frac{1}{N} \sum_{i=1}^N \text{Det}(y_o^{(i)}) \cdot \text{Abs}(y_c^{(i)}), \quad (9)$$

**Cold-start data.** SFT uses 500 detection examples (original image, ground-truth bounding box, and a rationale generated by Gemini 3.1 Flash-Lite [42] at temperature 0) and 500 abstention examples on the ObjectClear counterfactuals, giving a balanced 1,000-example corpus. Section V-A examines the detect-to-abstain ratio.

**Training.** For the same-backbone comparison, the base, SFT, and CFCamo variants build on Qwen3-VL-4B-Instruct [16]. The Qwen3-VL processor caps images at 768<sup>2</sup> pixels, and bounding boxes use the model’s native [0, 1000] coordinate range. SFT runs for one epoch with AdamW (lr  $2 \times 10^{-5}$ , effective batch 16). For RL, CSPO (Section III-D) optimizes the reward of Section III-C for half an epoch, with rollout group  $G=8$ , clip  $\epsilon=0.2$ , sampling temperature 1.0 and top- $p$  0.9, and greedy decoding at evaluation. The Full FT variant uses AdamW (lr  $10^{-6}$ , weight decay  $10^{-2}$ , global batch 32,  $\beta_{\text{kl}}=5 \times 10^{-2}$ ) on  $4 \times$  NVIDIA A800 (80 GB each). The LoRA variant uses rank 64,  $\alpha_{\text{lora}}=128$ , lr  $5 \times 10^{-6}$ , batch 16, and  $\beta_{\text{kl}}=10^{-2}$ , and trains on a single NVIDIA RTX PRO 6000 (96 GB) as a compute-efficient alternative. At inference, a frozen SAM2.1-hiera-large [13] decoder maps predicted boxes to masks, served by vLLM [48] with FlashAttention-2 [49]. The standard prompt  $P_{\text{std}}$  and the detect-or-abstain prompt  $P_{\text{da}}$  are listed in Appendix A.

### B. Standard COD Benchmark

**Quantitative Comparison.** Table I compares CFCamo against prior task-generic prompt COD methods. For a fair comparison, CFCamo is evaluated under the standard prompt

TABLE I

Quantitative comparison on three COD benchmarks. All listed methods follow the task-generic prompt setting; Seg-R1 and CFCamo are RL-based methods. Best score per metric in **bold**; our rows are shaded. <sup>†</sup>Seg-R1 numbers are obtained from our re-run under its native protocol.

Method	Venue	CAMO-test				CHAMELEON				COD10K-test			
		$S_\alpha \uparrow$	$E_\phi \uparrow$	$F_\beta^w \uparrow$	$M \downarrow$	$S_\alpha \uparrow$	$E_\phi \uparrow$	$F_\beta^w \uparrow$	$M \downarrow$	$S_\alpha \uparrow$	$E_\phi \uparrow$	$F_\beta^w \uparrow$	$M \downarrow$
GPT-4V+SAM [12], [50]	ICCV'23	.573	.666	.466	.206	.637	.710	.557	.180	.601	.672	.448	.187
SEEM [51]	NeurIPS'23	.404	.315	.023	.192	.454	.307	.011	.094	.425	.280	.001	.143
X-Decoder [52]	CVPR'23	.709	.745	.628	.104	.716	.748	.654	.124	.652	.705	.556	.171
LLaVA1.5+SAM [12], [53]	CVPR'24	.501	.585	.401	.314	.666	.718	.561	.168	.662	.728	.530	.170
Grounded SAM [54]	arXiv'24	.707	.753	.656	.157	.744	.776	.662	.122	.764	.813	.670	.085
GenSAM [20]	AAAI'24	.719	.775	.659	.113	.764	.807	.680	.090	.775	.838	.681	.067
ProMaC [21]	NeurIPS'24	.767	.846	.725	.090	.833	.899	.790	.044	.805	.876	.716	.042
CLIP-Surgery+SAM [12], [55]	PR'25	.612	.692	.520	.189	.689	.741	.606	.147	.629	.698	.488	.173
RDVP-MSD [22]	MM'25	.796	.848	.785	.081	.832	.904	.814	.040	.825	.877	.775	.038
Seg-R1-7B [14] <sup>†</sup>	NeurIPS-WS'25	.797	.843	.753	.098	.846	.896	.815	.083	.844	.888	.775	.055
<b>CFCamo-4B (Full FT)</b>	Ours	<b>.834</b>	<b>.884</b>	<b>.807</b>	<b>.059</b>	<b>.878</b>	<b>.927</b>	<b>.841</b>	<b>.033</b>	<b>.875</b>	<b>.930</b>	<b>.832</b>	<b>.027</b>
<b>CFCamo-4B (LoRA)</b>	Ours	.827	.882	.804	.070	<b>.878</b>	.926	<b>.842</b>	.034	<b>.875</b>	.928	<b>.832</b>	.031

<sup>†</sup>Seg-R1 originally released checkpoints and per-dataset numbers for CAMO-test and COD10K-test. For a matched comparison we re-ran its official checkpoint with the native prompt and 768×768 image-resize protocol on the same SAM2.1-hiera-large decoder and metric stack used for our rows.

TABLE II

Comparison on the CF-COD paired benchmark.  $D_o$  (%) is the detection rate on original images and  $A_c$  (%) the abstention rate on ObjectClear counterfactuals; PA (%) is the joint Pair Accuracy of Eq. (9). Best per metric in bold.

Method	Backbone	CAMO-test			CHAMELEON			COD10K-test		
		$D_o \uparrow$	$A_c \uparrow$	PA $\uparrow$	$D_o \uparrow$	$A_c \uparrow$	PA $\uparrow$	$D_o \uparrow$	$A_c \uparrow$	PA $\uparrow$
Base	Qwen3-VL-4B	68.0	92.0	60.8	88.2	97.4	85.5	73.9	88.7	64.6
SFT-only ( $r=1:1$ )	Qwen3-VL-4B	72.0	86.4	61.2	71.1	<b>100.0</b>	71.1	54.0	<b>96.0</b>	50.4
Seg-R1-7B [14]	Qwen2.5-VL-7B	78.4	67.2	51.6	89.5	79.0	72.4	81.2	62.1	48.5
<b>CFCamo-4B (Full FT)</b>	Qwen3-VL-4B	86.0	<b>92.8</b>	80.0	<b>93.4</b>	97.4	<b>90.8</b>	92.3	95.3	87.7
<b>CFCamo-4B (LoRA)</b>	Qwen3-VL-4B	<b>88.8</b>	92.4	<b>81.6</b>	<b>93.4</b>	97.4	<b>90.8</b>	<b>94.0</b>	94.2	<b>88.2</b>

$P_{\text{std}}$ , which requires every method to output a bounding box without any abstention option; invalid or empty predictions are treated as an all-zero mask when computing metrics. We report two variants: CFCamo-4B (Full FT) trained with full-parameter RL, and CFCamo-4B (LoRA) as a compute-efficient alternative.

The LoRA variant remains close to Full FT: it trails by 0.7 pp in  $S_\alpha$  on CAMO-test and is tied on CHAMELEON and COD10K-test, indicating that low-rank adaptation is competitive under this setting. Compared with the prior task-generic prompt baseline in Table I, RDVP-MSD [22], CFCamo-4B (Full FT) improves  $S_\alpha$  consistently, by +3.8 to +5.0 pp. Compared with Seg-R1-7B [14], the closest RL-based competitor, CFCamo-4B (Full FT) improves  $S_\alpha$  by +3.1 to +3.7 pp.

**Qualitative Comparison.** Fig. 4 shows a qualitative comparison of CFCamo (both variants) against leading task-generic prompt methods. In these examples, CFCamo produces masks that conform tightly to the camouflaged target, whereas Seg-R1-7B and RDVP-MSD frequently miss the object boundary or produce fragmented overlays. The LoRA outputs are visually close to Full FT across the four examples, supporting its role as a compute-efficient alternative.

### C. CF-COD Paired Benchmark

**Quantitative Comparison.** The standard COD results in Table I show strong target-present localization, but they do not test the complementary target-absent case. A model may still mark ordinary background regions as camouflaged objects on the counterfactual; such predictions are hallucinated target-present decisions on target-absent inputs. Table II therefore reports  $D_o$ ,  $A_c$ , and PA for the Qwen3-VL-4B-Instruct base, our 1,000-example cold-start SFT, Seg-R1-7B with an added `<no_camouflage/>` option, and both CFCamo variants.

Seg-R1-7B shows the over-detection pattern that CF-COD is designed to measure. On COD10K-test, for example,  $D_o$  is 81.2% while  $A_c$  is only 62.1%, yielding 48.5% PA; thus, only about half of the original-counterfactual pairs are judged correctly. The same direction appears on CAMO-test and CHAMELEON. The Qwen3-VL-4B-Instruct base shows the opposite asymmetry: on CAMO-test,  $D_o$  is 68.0% whereas  $A_c$  is 92.0%, so its PA mainly reflects over-abstention rather than balanced paired decisions. The base can emit either `<bbox>...</bbox>` or `<no_camouflage/>`, but it does not follow the full response schema: a `<think>...</think>` reasoning block

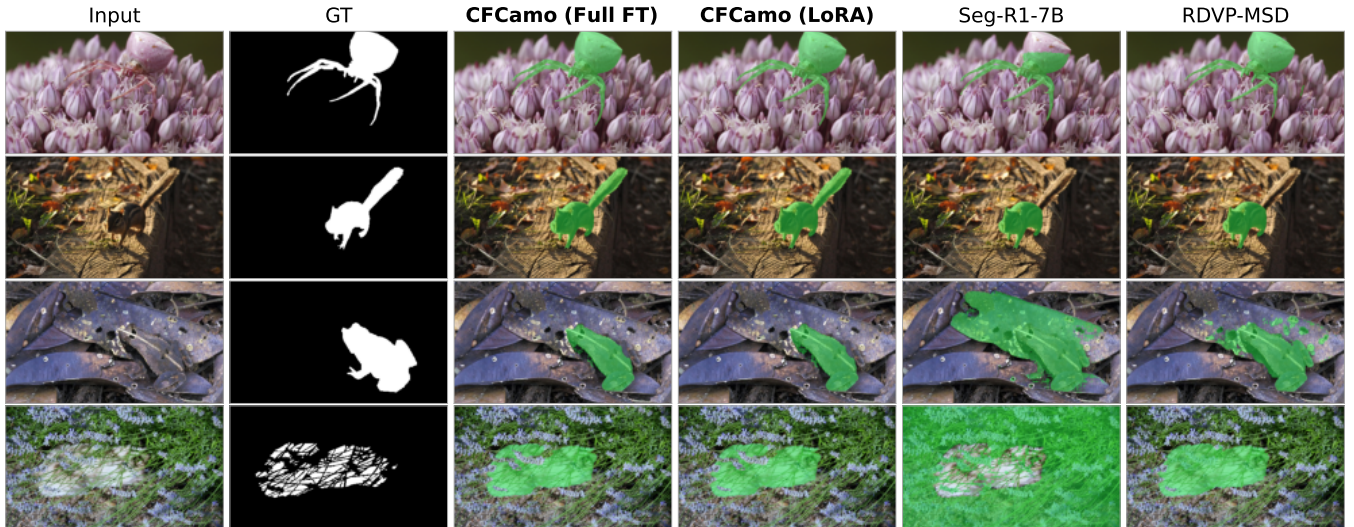


Fig. 4. Qualitative comparison of CFCamo (both variants) against leading task-generic prompt methods. Predicted masks are shown as green overlays.

followed by one of these decision tokens. Cold-start SFT aligns this schema; however, PA remains near the base on CAMO-test and drops on COD10K-test, indicating that format alignment alone is not enough to resolve the paired-decision imbalance (Section V-A).

Under CSPO,  $D_o$  and  $A_c$  increase together to 86–94% and 92–97%, respectively. CFCamo-4B (Full FT) reaches 87.7% PA on COD10K-test, gaining +39.2 pp over Seg-R1-7B, and 80.0% PA on CAMO-test, +19.2 pp over the base. The same-backbone ablation in Section V-B further separates the method design from backbone capacity: when the counterfactual coupling is removed, the same-backbone positive-only RL variant falls to 1.4–5.2% PA. The LoRA variant remains comparable to Full FT, showing that a parameter-efficient training setting can obtain similar paired-benchmark gains at lower training cost.

## V. ABLATION STUDY

### A. SFT Data Composition

Figure 5 asks whether the paired-decision asymmetry in Table II can be corrected by changing SFT data composition alone. We keep the SFT corpus size fixed at 1,000 examples and retrain five models with detect-to-abstain ratios from 3:1 to 1:3. The balanced model in Table II is the 1:1 point in this sweep.

Changing the SFT ratio mainly moves the model along a detection-abstention trade-off. As the ratio shifts from 3:1 to 1:3,  $D_o$  falls from 90.4% to 16.4%, while  $A_c$  rises from 49.2% to 100.0%. PA therefore forms an inverted-U curve, peaking at 59.2% at the balanced ratio, still below the 80–91% range reached by full CFCamo in Table II. Format validity remains above 98% for all five ratios, so the cold-start stage has already learned the response schema. The limiting factor is therefore not schema acquisition, but the independent SFT objective, which shifts the decision bias toward one side of the pair. Section V-B therefore examines whether a paired RL reward can optimize detection and abstention jointly.

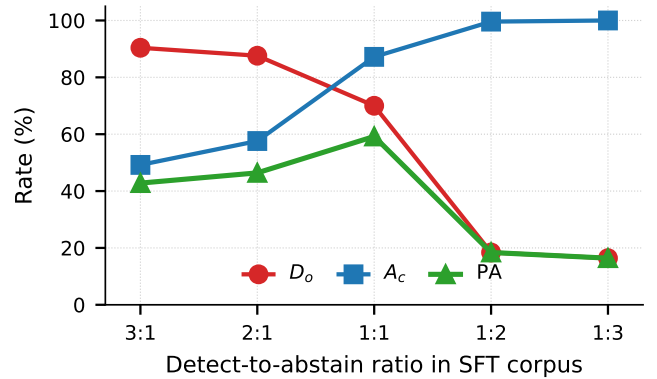


Fig. 5. SFT detection-abstention trade-off on CAMO-test under five detect-to-abstain ratios at fixed corpus size (1,000). Detection rate  $D_o$  and abstention rate  $A_c$  move in opposite directions, and PA peaks at the balanced setting.

TABLE III

CF-COD paired ablation of the coupling and mask-reward components under CSPO, with the same CFCamo-4B (LoRA) training setup as Table II.  $D_o$ ,  $A_c$ , and PA are paired-decision rates (%). Best values are bolded within each dataset and metric.

Variant	Dataset	$D_o \uparrow$	$A_c \uparrow$	PA $\uparrow$
<b>CFCamo-4B (LoRA)</b>	CAMO-test	88.8	92.4	<b>81.6</b>
	CHAMELEON	93.4	<b>97.4</b>	90.8
	COD10K-test	94.0	94.2	<b>88.2</b>
w/o CF coupling	CAMO-test	<b>99.6</b>	5.2	5.2
	CHAMELEON	<b>100.0</b>	2.6	2.6
	COD10K-test	<b>99.9</b>	1.4	1.4
w/o SAM mask	CAMO-test	82.8	<b>95.6</b>	78.8
	CHAMELEON	94.7	<b>97.4</b>	<b>92.1</b>
	COD10K-test	92.2	<b>95.5</b>	87.7

### B. Reward Component Ablation

To isolate the roles of the counterfactual coupling and the SAM mask reward within CSPO (Section III-D), we train two

TABLE IV

Standard COD ablation of the coupling and mask-reward components under CSP0, evaluated with the  $P_{\text{std}}$  force-detect prompt, same setup as Table III. Best values are bolded within each dataset and metric.

Variant	Dataset	$S_\alpha \uparrow$	$E_\phi \uparrow$	$F_\beta^w \uparrow$	$M \downarrow$
<b>CFCamo-4B (LoRA)</b>	CAMO-test	<b>.827</b>	<b>.882</b>	<b>.804</b>	.070
	CHAMELEON	<b>.878</b>	<b>.926</b>	.842	<b>.034</b>
	COD10K-test	.875	.928	.832	.031
w/o CF coupling	CAMO-test	.826	.880	.792	<b>.063</b>
	CHAMELEON	.875	.916	.840	.040
	COD10K-test	<b>.879</b>	<b>.932</b>	<b>.833</b>	<b>.023</b>
w/o SAM mask	CAMO-test	.814	.870	.796	.085
	CHAMELEON	.876	.920	<b>.845</b>	.042
	COD10K-test	.867	.917	.822	.040

ablations with the same LoRA setup as CFCamo-4B (LoRA). The **w/o CF coupling** variant removes the counterfactual branch, yielding positive-only RL on original images. The **w/o SAM mask** variant keeps paired counterfactual training but replaces the SAM2-decoded mask IoU with a plain bounding-box IoU. Table III evaluates paired decisions on CF-COD, and Table IV evaluates the same checkpoints under the standard COD prompt.

The first ablation shows why target-present COD scores alone are incomplete for this problem. Without CF coupling, the model almost always detects on natural images:  $D_o$  reaches 99.6–100.0%. This behavior can look favorable under the standard force-detect protocol, where every test image contains a target; indeed, the same checkpoint matches CFCamo-4B (LoRA) within 0.004  $S_\alpha$  and gives the best COD10K-test standard scores. However, the same policy does not transfer to counterfactual images:  $A_c$  remains at 1.4–5.2%, keeping PA low. In other words, the strong standard-COD numbers partly reflect over-detection rather than balanced paired reasoning.

The SAM mask reward affects a different part of the behavior. Removing it keeps PA within 2.8 pp of CFCamo-4B (LoRA), but lowers standard mask quality, with  $S_\alpha$  lower by 0.013 on CAMO-test and 0.008 on COD10K-test. Thus, CF coupling supplies the target-absent constraint needed for paired decision behavior, whereas the SAM mask reward mainly improves the segmentation quality of detected objects.

### C. Training Trajectory and Schema Stability

Figure 6 traces CAMO-test PA and schema-valid response rate along the RL trajectory. At the half-epoch budget, the LoRA and Full FT variants reach similar CAMO-test PA (81.6% and 80.0%, respectively), while both retain fully valid output schemas. This supports the matched-budget comparison used for the main results: low-rank adaptation can reach the same performance regime as full-parameter training before longer optimization changes the response format.

Continuing training reveals the stability difference. The LoRA trajectory remains near its PA peak shortly after  $\varepsilon=0.5$ , but its schema-valid response rate decreases after  $\varepsilon \approx 0.6$ , falling from 100% to 54.4% and then to 3.0% by the end of the epoch. Full FT shows a smaller PA decline and keeps schema validity at or above 96% throughout the same interval. Thus,

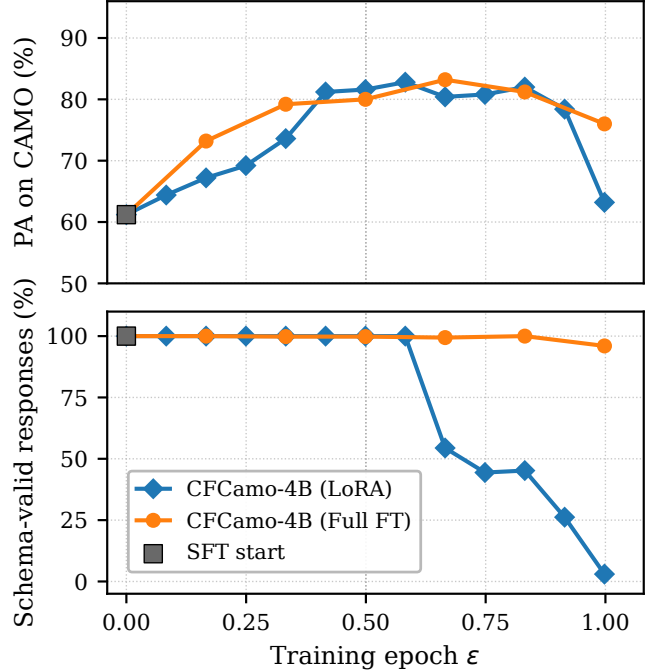


Fig. 6. Training trajectory on CAMO-test under  $P_{\text{da}}$ . Top: PA over training epoch  $\varepsilon$ ;  $\varepsilon=0.5$  corresponds to the half-epoch budget (4040 image-views), and  $\varepsilon=1.0$  to one epoch (8080 image-views). Bottom: schema-valid response rate, measuring whether the output keeps the required reasoning block and terminal decision token.

the late-stage LoRA drop is better interpreted as response-schema drift rather than lost localization, and the paired benchmark makes this distinction measurable.

The trajectory also reveals a useful separation between paired-decision learning and response-schema stability. The lightweight format term acts as a schema regularizer, while the larger decision rewards drive the detect-or-abstain behavior. After the paired decision has largely converged, continued LoRA updates can therefore reveal schema drift even when the underlying localization signal remains recoverable. Manual inspection supports this interpretation: many late LoRA responses still contain plausible boxes, but omit the opening `<think>` tag, for example producing a closing `</think>` tag before an otherwise recoverable bounding-box decision. Others deviate from the required tag structure in similar ways. This observation motivates using schema validity as a trajectory diagnostic when selecting the half-epoch checkpoint, alongside PA and standard mask quality.

### D. General Multimodal Benchmarks

Figure 7 asks whether the COD-specific RL stage introduces a measurable loss on general multimodal tasks. We evaluate CFCamo on four multimodal benchmarks: POPE [33], MME [56], MMBench [57], and AI2D [58], all under VLMEvalKit [59]. The comparison uses the same vLLM stack and the same benchmark-specific prompt for all models, without exposing the CFCamo detect-or-abstain schema. These benchmarks therefore serve as a regression check for general

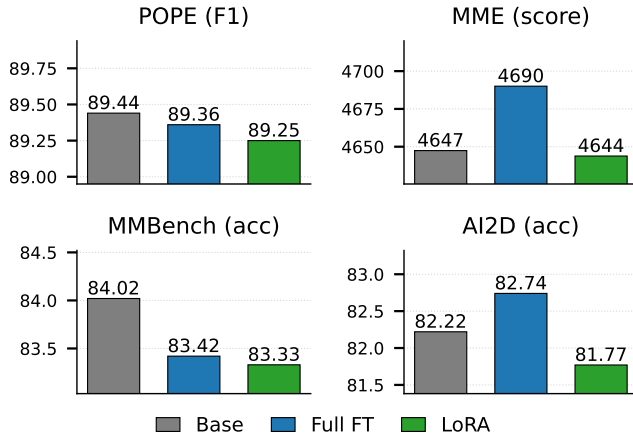


Fig. 7. Absolute scores on four multimodal benchmarks for the Qwen3-VL-4B-Instruct base and both CFCamo variants. Note the zoomed vertical axes: across all four benchmarks every variant stays within 1% (relative) of the base model, so the differences are marginal.

perception, reasoning, multiple-choice question answering, and object-hallucination behavior.

Both CFCamo variants remain close to the Qwen3-VL-4B-Instruct base. On the percentage-based metrics, the largest change is the LoRA model’s 0.69 pp drop on MMBench; POPE and AI2D vary by at most 0.19 and 0.52 pp, respectively. On MME, Full FT improves by 42.6 points (0.9% relative), while LoRA changes by less than 0.1% relative to the base. Thus, the paired COD improvements in Sections IV and V-B do not come with an observable degradation on these multimodal checks.

## VI. CONCLUSION

This study introduces CFCamo and revisits camouflaged object detection as a paired counterfactual problem. We argue that positive-only COD training leaves target-absent behavior untested, even though ordinary target-absent scenes are common deployment inputs. To make this behavior measurable, we construct CF-COD, a paired detect-or-abstain benchmark where each held-out COD image is paired with a target-absent counterpart synthesized by an off-the-shelf inpainter. To reduce over-detection, CSPO uses paired counterfactual rollouts, a paired sequence ratio extending GSPO, and CPR, which couples original-image detection with counterfactual abstention through detection and abstention indicators plus a pair-level coupling bonus.

Empirically, CFCamo improves standard COD performance, strengthens paired decisions on CF-COD, and shows no observable degradation on the evaluated multimodal benchmarks.

Future work can further study robustness to the quality of synthesized target-absent images, extend the same paired formulation to video COD with temporal counterfactuals, and explore broader grounding tasks where target existence is uncertain.

## APPENDIX A PROMPT TEMPLATES

We use two prompt templates. The detect-or-abstain prompt  $P_{da}$  is used for all RL training and for the CF-COD paired evaluation. The standard prompt  $P_{std}$  is used only for the prior-art comparison in Table I, where existing methods cannot abstain. Both templates use Qwen3-VL’s native  $[0, 1000]$  coordinate normalization [16]. The two templates differ only in the `<no_camouflage/>` option and the assertion of target presence in  $P_{std}$ .

### $P_{da}$ — system message.

You are a camouflaged object detector. Output in this exact format:

```
<think>your reasoning here</think>
followed by ONE of:
- <bbox>[x1,y1,x2,y2]</bbox> for a single
  object
- <bbox>[[x1,y1,x2,y2],[x3,y3,x4,y4]]</bbox> for
  multiple
- <no_camouflage/> if none is
  present
Coordinates are normalized to [0, 1000] where 1000 = full
image dimension.
```

### $P_{da}$ — user message.

```
Identify and locate any camouflaged object in the image.
In <think></think>, briefly consider scene textures, visual
anomalies, and if any object blends in. Then output ONE
of:
- <bbox>[x1,y1,x2,y2]</bbox> for one object, or [[x1,y1,x2,
  y2],...] for multiple
- <no_camouflage/> if no camouflaged object
```

### $P_{std}$ — system message.

```
You are a camouflaged object detector. There IS a
camouflaged object in this image. Locate it precisely.
Output in this exact format:
<think>your reasoning here</think>
followed by ONE of:
- <bbox>[x1,y1,x2,y2]</bbox> for a single
  object
- <bbox>[[x1,y1,x2,y2],[x3,y3,x4,y4]]</bbox> for
  multiple
Coordinates are normalized to [0, 1000] where 1000 = full
image dimension.
```

### $P_{std}$ — user message.

```
Identify and locate the camouflaged object in the image.
In <think></think>, briefly consider scene textures and
visual anomalies, then output:
- <bbox>[x1,y1,x2,y2]</bbox> for one object, or [[x1,y1,x2,
  y2],...] for multiple
```

## APPENDIX B SFT RATIO SWEEP DATA

TABLE V

Data underlying Fig. 5: SFT ratio sweep on CAMO-test (250 paired images,  $P_{da}$ ,  $T=0$  greedy).  $D_o$ ,  $A_c$ , and PA are paired-decision rates (%); Fmt is the format-validity rate (%), per the indicator defined in Section III-C. The 1:1 row is the balanced SFT used as cold-start for CFCamo in the main paper.

Ratio (det:abs)	$D_o \uparrow$	$A_c \uparrow$	PA $\uparrow$	Fmt $\uparrow$
3:1 (detect-heavy)	90.4	49.2	42.8	98.4
2:1	87.6	57.6	46.4	99.4
<b>1:1 (balanced)</b>	<b>70.0</b>	<b>87.2</b>	<b>59.2</b>	<b>100.0</b>
1:2	18.4	99.6	18.4	100.0
1:3 (abstain-heavy)	16.4	100.0	16.4	99.8

## REFERENCES

- [1] M. Stevens and S. Merilaita, “Animal camouflage: Current issues and new perspectives,” *Philos. Trans. R. Soc. B*, vol. 364, no. 1516, pp. 423–427, 2009.
- [2] H. B. Cott, *Adaptive Coloration in Animals*. London, U.K.: Methuen, 1940.
- [3] D.-P. Fan, G.-P. Ji, G. Sun, M.-M. Cheng, J. Shen, and L. Shao, “Camouflaged Object Detection,” in *Proc. CVPR*, 2020, pp. 2774–2784.
- [4] D.-P. Fan, G.-P. Ji, M.-M. Cheng, and L. Shao, “Concealed Object Detection,” *IEEE Trans. Pattern Anal. Mach. Intell.*, vol. 44, no. 10, pp. 6024–6042, 2022.
- [5] D.-P. Fan *et al.*, “PraNet: Parallel Reverse Attention Network for Polyp Segmentation,” in *Proc. MICCAI*, 2020, pp. 263–273.
- [6] R. Pérez-de la Fuente *et al.*, “Early evolution and ecology of camouflage in insects,” *Proc. Natl. Acad. Sci. USA*, vol. 109, no. 52, pp. 21 414–21 419, 2012.
- [7] D. Tabernik, S. Šela, J. Skvarč, and D. Skočaj, “Segmentation-based deep-learning approach for surface-defect detection,” *J. Intell. Manuf.*, vol. 31, no. 3, pp. 759–776, 2020.
- [8] H. Mei, G.-P. Ji, Z. Wei, X. Yang, X. Wei, and D.-P. Fan, “Camouflaged Object Segmentation with Distraction Mining,” in *Proc. CVPR*, 2021, pp. 8768–8777.
- [9] Y. Sun, S. Wang, C. Chen, and T.-Z. Xiang, “Boundary-Guided Camouflaged Object Detection,” in *Proc. IJCAI*, vol. 2, 2022, pp. 1335–1341.
- [10] X. Hu *et al.*, “High-resolution iterative feedback network for camouflaged object detection,” in *Proc. AAAI*, vol. 37, 2023, pp. 881–889.
- [11] Y. Pang, X. Zhao, T.-Z. Xiang, L. Zhang, and H. Lu, “ZoomNeXt: A Unified Collaborative Pyramid Network for Camouflaged Object Detection,” *IEEE Trans. Pattern Anal. Mach. Intell.*, vol. 46, no. 12, pp. 9205–9220, 2024.
- [12] A. Kirillov *et al.*, “Segment Anything,” in *Proc. ICCV*, 2023, pp. 3992–4003.
- [13] N. Ravi *et al.*, “SAM 2: Segment Anything in Images and Videos,” in *Proc. ICLR*, 2025.
- [14] Z. You, “Seg-R1: Segmentation Can Be Surprisingly Simple with Reinforcement Learning,” in *Proc. NeurIPS Workshop on VLM4RWD*, 2025.
- [15] J. Zhao, Z. Wang, P. Yang, and S. Zhou, “Precise Object and Effect Removal with Adaptive Target-Aware Attention,” in *Proc. CVPR*, 2026.
- [16] S. Bai *et al.*, “Qwen3-VL Technical Report,” 2025.
- [17] T.-N. Le, T. V. Nguyen, Z. Nie, M.-T. Tran, and A. Sugimoto, “Anabranch network for camouflaged object segmentation,” *Comput. Vis. Image Underst.*, vol. 184, pp. 45–56, 2019.
- [18] S. Zhang *et al.*, “Frequency-Guided Spatial Adaptation for Camouflaged Object Detection,” *IEEE Trans. Multimedia*, vol. 27, pp. 72–83, 2025.
- [19] J. Yang, B. Zhong, Q. Liang, Z. Mo, S. Zhang, and S. Song, “Uncertainty-Guided Diffusion Model for Camouflaged Object Detection,” *IEEE Trans. Multimedia*, vol. 27, pp. 4656–4669, 2025.
- [20] J. Hu, J. Lin, S. Gong, and W. Cai, “Relax image-specific prompt requirement in SAM: A single generic prompt for segmenting camouflaged objects,” in *Proc. AAAI*, vol. 38, 2024, pp. 12 511–12 518.
- [21] J. Hu, J. Lin, J. Yan, and S. Gong, “Leveraging Hallucinations to Reduce Manual Prompt Dependency in Promptable Segmentation,” in *Proc. NeurIPS*, 2024.
- [22] C. Yin, H. Li, K. Yang, J. Li, P. Zhu, and X. Li, “Stepwise Decomposition and Dual-stream Focus: A Novel Approach for Training-free Camouflaged Object Segmentation,” in *Proc. ACM MM*, 2025, pp. 3741–3750.
- [23] X. Lai *et al.*, “LISA: Reasoning Segmentation via Large Language Model,” in *Proc. CVPR*, 2024, pp. 9579–9589.
- [24] H. Rasheed *et al.*, “GLaMM: Pixel Grounding Large Multimodal Model,” in *Proc. CVPR*, 2024, pp. 13 009–13 018.
- [25] Z. Ren *et al.*, “PixelLM: Pixel Reasoning with Large Multimodal Model,” in *Proc. CVPR*, 2024, pp. 26 364–26 373.
- [26] T. Zhang *et al.*, “OMG-LLaVA: Bridging Image-level, Object-level, Pixel-level Reasoning and Understanding,” in *Proc. NeurIPS*, 2024.
- [27] T.-H. Wu *et al.*, “See Say and Segment: Teaching LLMs to Overcome False Premises,” in *Proc. CVPR*, 2024, pp. 13 459–13 469.
- [28] Z. Shao *et al.*, “DeepSeekMath: Pushing the Limits of Mathematical Reasoning in Open Language Models,” 2024.
- [29] Y. Liu *et al.*, “Seg-Zero: Reasoning-Chain Guided Segmentation via Cognitive Reinforcement,” 2025.
- [30] J. Huang *et al.*, “SAM-R1: Leveraging SAM for Reward Feedback in Multimodal Segmentation via Reinforcement Learning,” in *Proc. NeurIPS*, 2025.
- [31] Y. Liu *et al.*, “VisionReasoner: Unified Reasoning-Integrated Visual Perception via Reinforcement Learning,” in *Proc. ICLR*, 2026.
- [32] L. Zhu *et al.*, “LENS: Learning to Segment Anything with Unified Reinforced Reasoning,” *Proc. AAAI*, vol. 40, no. 16, pp. 13 952–13 960, 2026.
- [33] Y. Li, Y. Du, K. Zhou, J. Wang, X. Zhao, and J.-R. Wen, “Evaluating Object Hallucination in Large Vision-Language Models,” in *Proc. EMNLP*, 2023, pp. 292–305.
- [34] M. Ye-Bin, N. Hyeon-Woo, W. Choi, and T.-H. Oh, “BEAF: Observing Before-After Changes to Evaluate Hallucination in Vision-Language Models,” in *Proc. ECCV*, 2025, pp. 232–248.
- [35] Z. Wang, G. Bingham, A. W. Yu, Q. V. Le, T. Luong, and G. Ghiasi, “HaloQuest: A Visual Hallucination Dataset for Advancing Multimodal Reasoning,” in *Proc. ECCV*, 2024, pp. 288–304.
- [36] T.-H. Wu, H. Lee, J. Ge, J. E. Gonzalez, T. Darrell, and D. M. Chan, “Generate, but Verify: Reducing Hallucination in Vision-Language Models with Retrospective Resampling,” in *Proc. NeurIPS*, 2025.
- [37] Z. Wang *et al.*, “Perception-Aware Policy Optimization for Multimodal Reasoning,” in *Proc. ICLR*, 2026.
- [38] X. Li *et al.*, “Counterfactual Segmentation Reasoning: Diagnosing and Mitigating Pixel-Grounding Hallucination,” 2026.
- [39] H. Dastmalchi, A. An, A. Cheraghian, and H. Barzamini, “Fighting Hallucinations with Counterfactuals: Diffusion-Guided Perturbations for LVLm Hallucination Suppression,” in *Proc. CVPR*, 2026.
- [40] A. Bhattad, K. Preechakul, and A. A. Efros, “Visual Jenga: Discovering Object Dependencies via Counterfactual Inpainting,” in *Proc. NeurIPS*, 2025.
- [41] C. Zheng *et al.*, “Group Sequence Policy Optimization,” 2025.
- [42] Google DeepMind, “Gemini 3.1 flash-lite model card,” <https://storage.googleapis.com/deepmind-media/Model-Cards/Gemini-3-1-Flash-Lite-Model-Card.pdf>, Mar. 2026, accessed: 2026-05-18.
- [43] P. Skurowski, H. Abdulameer, J. Błaszczyk, T. Depta, A. Kornacki, and P. Koziel, “Animal camouflage analysis: Chameleon database,” *Unpublished manuscript*, vol. 2, no. 6, p. 7, 2018.
- [44] D.-P. Fan, M.-M. Cheng, Y. Liu, T. Li, and A. Borji, “Structure-Measure: A New Way to Evaluate Foreground Maps,” in *Proc. ICCV*, 2017, pp. 4548–4557.
- [45] D.-P. Fan, C. Gong, Y. Cao, B. Ren, M.-M. Cheng, and A. Borji, “Enhanced-alignment measure for binary foreground map evaluation,” in *Proc. IJCAI*, 2018, pp. 698–704.
- [46] R. Margolin, L. Zelnik-Manor, and A. Tal, “How to Evaluate Foreground Maps,” in *Proc. CVPR*, 2014, pp. 248–255.
- [47] F. Perazzi, P. Krähenbühl, Y. Pritch, and A. Hornung, “Saliency filters: Contrast based filtering for salient region detection,” in *Proc. CVPR*, 2012, pp. 733–740.
- [48] W. Kwon *et al.*, “Efficient Memory Management for Large Language Model Serving with PagedAttention,” in *Proc. SOSP*, 2023, pp. 611–626.
- [49] T. Dao, “FlashAttention-2: Faster Attention with Better Parallelism and Work Partitioning,” in *Proc. ICLR*, 2024.
- [50] OpenAI, “GPT-4V(ision) System Card,” [https://cdn.openai.com/papers/GPTV\\_System\\_Card.pdf](https://cdn.openai.com/papers/GPTV_System_Card.pdf), Sep. 2023, accessed: 2026-05-22.
- [51] X. Zou *et al.*, “Segment everything everywhere all at once,” in *Proc. NeurIPS*, 2023, pp. 19 769–19 782.
- [52] X. Zou *et al.*, “Generalized Decoding for Pixel, Image, and Language,” in *Proc. CVPR*, 2023, pp. 15 116–15 127.
- [53] H. Liu, C. Li, Y. Li, and Y. J. Lee, “Improved Baselines with Visual Instruction Tuning,” in *Proc. CVPR*, 2024, pp. 26 286–26 296.
- [54] T. Ren *et al.*, “Grounded SAM: Assembling Open-World Models for Diverse Visual Tasks,” 2024.
- [55] Y. Li, H. Wang, Y. Duan, J. Zhang, and X. Li, “A closer look at the explainability of Contrastive language-image pre-training,” *Pattern Recognit.*, vol. 162, p. 111409, 2025.
- [56] C. Fu *et al.*, “MME: A Comprehensive Evaluation Benchmark for Multimodal Large Language Models,” in *Proc. NeurIPS Datasets and Benchmarks Track*, 2025.
- [57] Y. Liu *et al.*, “MMBench: Is Your Multi-modal Model an All-Around Player?” in *Proc. ECCV*, 2024, pp. 216–233.
- [58] A. Kembhavi, M. Salvato, E. Kolve, M. Seo, H. Hajishirzi, and A. Farhadi, “A Diagram is Worth a Dozen Images,” in *Proc. ECCV*, 2016, pp. 235–251.
- [59] H. Duan *et al.*, “VLM EvalKit: An Open-Source Toolkit for Evaluating Large Multi-Modality Models,” in *Proc. ACM MM*, 2024, pp. 11 198–11 201.